JOURNAL OF THE KOREAN ASTRONOMICAL SOCIETY
27: 45 ~ 53, 1994

# MONTE CARLO SIMULATION OF COMPTONIZATION IN A SPHERICAL SHELL GEOMETRY

SEON, KWANG IL AND MIN, KYOUNG-WOOK
Department of Physics, Korea Advanced Institute of Science and Technology
373-1 Gusong-dong, Yuseong, Taejeon 305-701, Korea
E-mail: kwmin@convex. kaist. ac. kr
AND
CHOI, CHUL SUNG AND NAM, UK WON
Korea Astronomy Observatory
36-1 Whaam-dong, Yuseong, Taejeon 305-348, Korea
E-mail: cschoi@hanul. issa. re. kr
(*Received Apr. 1, 1994; Accepted Apr. 15, 1994*)

## ABSTRACT

We present the calculation of X-ray spectra produced through Compton scattering of soft X-rays by hot electrons in the spherical shell geometry, using fully relativistic Monte Carlo simulation. With this model, we show that the power-law component, which has been observed in the low luminosity state of low-mass X-ray binaries (LMXBs), is explained physically. From a spectral analysis, we find that spectral hardness is mainly due to the relative contribution of scattered component. In addition, we see that Wien spectral features appear when the plasma is optically thick, especially in the high energy range, $E \gtrsim 100$keV. We suggest that after a number of scattering the escape probability approaches an asymptotic form depending on the geometry of the scattering medium rather than on the initial photon spectrum.

*Key Words* : X-ray spectra, X-ray binary, neutron star, radiative transfer

## I. INTRODUCTION

It is widely accepted that X-ray photons emanating from compact X-ray sources gain their energy through Compton scattering when a hot and optically thick gas is distributed around the X-ray sources. The change of an initial X-ray spectrum by the process is called "Comptonization". This matter has been considered important in LMXBs as well as in black hole candidates (Zeldovich & Shakura 1969; Felten & Rees 1972). Ponman, Foster & Ross (1990) have presented some evidences indicating the existence of substantial scattering depth of highly ionized plasma in various LMXBs, where the systems consist of a weakly or non-magnetized neutron star and a late-type companion star. King & Lasota (1987) showed that an ion-supported corona is likely to be produced when material accretes onto the neutron star from an inner accretion disk edge. According to the X-ray observations (e.g., Parmar, Stella & White 1986), X-ray spectra of some LMXBs are well represented by a power-law model in the case of low luminosity ($\leq 10^{35}$ergs $s^{-1}$).

Radiative transfer equation for the Compton scattering can be solved analytically in the non-relativistic case, if we use the kinetic equation of Fokker-Planck form and diffusion approximation (Kompaneets 1957; Katz 1976; Sunyaev & Titarchuk 1980). However, in the relativistic regime ($kT_e \gtrsim m_e c^2$), Monte Carlo simulation is

necessary to solve the problem because the approximations are not valid. The radiative transfer problem has been studied using Monte Carlo simulation by several works with the following models: a cold plasma shell surrounding an isotropic hard X-ray source (Langer, Ross & McCray 1978), a plasma sphere of weakly relativistic and relativistic electrons (Pozdnyakov, Sobol' & Sunyaev 1983), and a reflection of X-ray by a cold planar matter (George & Fabian 1991; Matt, Perola & Piro 1991).

The present work is intended to model the X-ray spectra from LMXBs, using the spherical shell geometry of hot plasma. The contribution of Compton scattering on the X-ray spectra is investigated qualitatively through Monte Carlo simulation with the model. In addition, we consider also a simple sphere model to check the geometrical effects.

## II. MONTE CARLO SIMULATION

### (a) Theory

In the present study, the calculations for the Compton scattering are performed relativistically without consideration of the magnetic field. As a photon that has an initial energy $E$ and momentum $(E/c)\Omega$ is scattered into the direction of solid angle $\Omega'$ by an electron of the velocity $\mathbf{v}=\beta c$, its new energy $E'$ becomes

$$\frac{E'}{E}=\frac{1-\Omega\cdot\beta}{1-\Omega'\cdot\beta+(E/\gamma m_e c^2)(1-\Omega\cdot\Omega')}, \tag{1}$$

where $\gamma=1/(1-\beta^2)^{1/2}$. In the laboratory frame, the differential cross-section for the scattering, when the relativistic effect is taken into account, is expressed as (Babuel-Peyrissac & Rouvillois 1969)

$$\frac{d\sigma}{d\Omega'}=\frac{r_e^2}{2\gamma^2}\frac{X}{1-\Omega\cdot\beta}\left(\frac{E'}{E}\right)^2, \tag{2}$$

where $r_e=e^2/m_e c^2$ is the classical electron radius and

$$X=\frac{x'}{x}+\frac{x}{x'}+2\left(\frac{1}{x}-\frac{1}{x'}\right)+\left(\frac{1}{x}-\frac{1}{x'}\right)^2,$$

$$x\equiv\frac{E}{m_e c^2}\gamma(1-\Omega\cdot\beta),\ x'\equiv\frac{E'}{m_e c^2}\gamma(1-\Omega'\cdot\beta).$$

The scattering probability within a path length $dl$ is expressed as (Landau & Lifshits 1976)

$$P_s(l)dl=\int(1-\Omega\cdot\beta)\sigma(x)N_e(\mathbf{v})d\mathbf{v}dl, \tag{3}$$

where $\sigma(x)$ and $N_e(\mathbf{v})$ are the total cross-section and the electron velocity-distribution function, respectively.

### (b) Models and Method

Two geometries of the plasma, a spherical shell and a sphere, are considered in this study. Figure 1 shows schematic configuration of the models. In the shell model, X-ray photons are isotropically injected from the neutron star surface. Some of them are backscattered into the neutron star and absorbed. Such photons are considered as being lost from the system. On the other hand, the photons in the sphere model are radiated isotropically from the center of the sphere. We follow trajectories of $1\times10^5$ photons for the shell model and $2\times10^4$ photons for the sphere model, respectively. We establish both the temperature and the density in the models are uniform. The electron temperature of the plasma is taken as 100keV, which is typical in both LMXBs and Galactic black hole candidates (Shapiro, Lightman & Eardley 1976; King & Lasota 1987; Haardt *et al.* 1993).

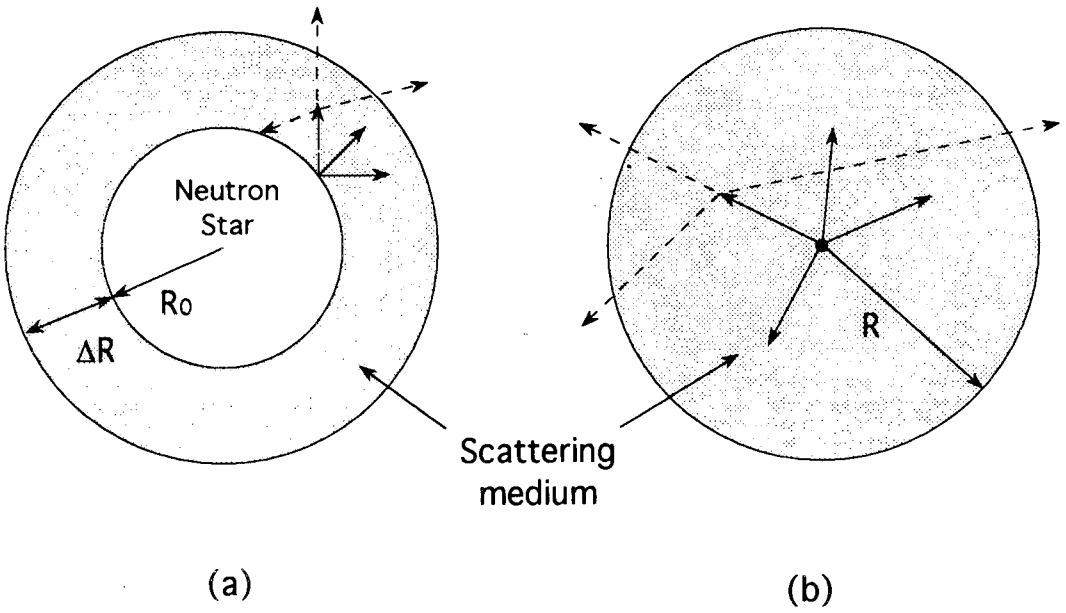


**Fig. 1.** Schematic configuration of the present models. The geometries of the scattering medium are the spherical shell (a) and the sphere (b), respectively. The geometrical depth of the shell is $\Delta R = 0.1 R_0$. Thus the scattering depth can be defined as $\tau = n_e \sigma_T \Delta R$, where $n_e$ and $\sigma_T$ are, respectively, the electron number density and the Thomson scattering cross section. In the simple sphere geometry, the scattering depth is defined as $\tau = n_e \sigma_T R$, where $R$ is the radius of the sphere.

In the present simulation, each photon represents many photons in proportion to its "weight", which is reduced continuously according to the remaining probability in the scattering medium. A photon of the initial energy $E_0$ and weight $w_0 = 1$ is injected from an initial point with some angle. Then the new energy and the direction after being scattered are selected again based on the differential cross section. The remaining probability of the photon for further scattering is $1 - P_0$, and the weight is $w_1 = w_0 (1 - P_0)$, where $P_0$ denotes the escape probability without any scattering. This process is then repeated. The escape probability after $i$th scattering is $P_i = \exp(-l_i / \bar{\lambda}_i)$, where $l_i$ and $\bar{\lambda}_i$ are the distance to the boundary layer of the medium and the mean free path, respectively. Therefore, each photon contributes to the emergent spectrum an amount equal to $w_i P_i$.

## III. RESULTS

The obtained X-ray spectra from the spherical shell plasma are presented in Fig. 2 for various values of the scattering depth $\tau$. Individual spectrum of the Figure is normalized by the input X-ray photons. The initial soft X-ray is assumed to be monochromatic $E_0 = 0.1$keV. From the result, we note that the spectrum flattens out gradually as the scattering depth increases. It approaches to a Wien spectrum $N_E$ (photons/keV) $\sim E^2 \exp(-E/kT_e)$ for $\tau > 3$, due to distortion of the high-energy part. The Wien hump is apparent at around 300keV for the sufficiently high scattering depth $\tau = 5$. In the typical observation range of 1-10keV, however, we find that the spectra shown in Fig. 2 are represented well by the power-law model $N_E \propto E^{-\alpha}$. Table 1 summarizes the calculated power-law photon index $\alpha$ over the scattering depth $\tau$. We checked how the number of scattering affects the spectral deformation. Figure 3 indicates the contribution to the energy spectrum of $\tau = 1$: the scattered component becomes broader and lower, as the number of scattering increases. Subsequently, we calculated the emergent spectrum with the initial blackbody spectrum of $kT_b = 2$keV. Figure 4 shows the results, in which the model and the parameters are same as in Fig. 2. The spectra reveal the following features:

(1) power law components appear above~10keV, while the spectra are similar to the blackbody one in the low -energy, (2) the Wien hump is also evident at~300keV in the case of $\tau=5$. Since the energy gain after single scattering is approximated to $\Delta E/E\sim kT_e/m_ec^2$, a photon that has higher energy can be scattered easily up to the hump energy of $3\sim4kT_e$. Thus the hump amplitude resulting from the blackbody spectrum is higher than that of the monochromatic case.

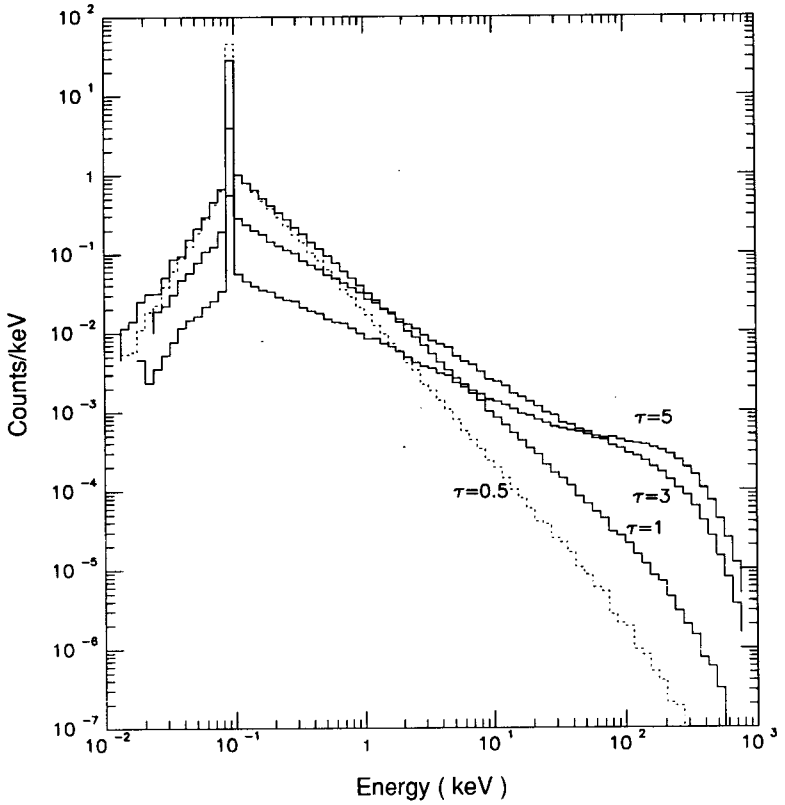


**Fig. 2.** Comptonized spectra of the monochromatic photons with $E_0=0.1$keV emerging from the spherical shell plasma. The electron temperature is taken as 100keV. The photons emerging from the plasma are accumulated into the energy channels with the interval of $\Delta\log E=0.075$. The individual spectrum is normalized by the input photons.

**Table 1.** The spectral power-law indices $\alpha$ over the scattering depths $\tau$

| $\tau$ | $\alpha$[a] | |
|---|---|---|
| | shell | sphere |
| 0.5 | 2.00 | 2.24 |
| 1.0 | 1.58 | 1.77 |
| 3.0 | 1.06 | 1.13 |
| 5.0 | 0.78 | 0.86 |

[a]The power-law indices are calculated in the energy range of 1-10keV.

We consider here the simple sphere model in order to investigate the geometrical effects in between the shell and the sphere model. The obtained X-ray spectra from the sphere are shown in Fig. 5, where the monochromatic input spectrum of $E_0=0.1$keV is assumed. Each spectrum of the Figure is normalized as same in Fig. 2. The result exhibits that the spectral shape could be described also with the simple power-law model, but the

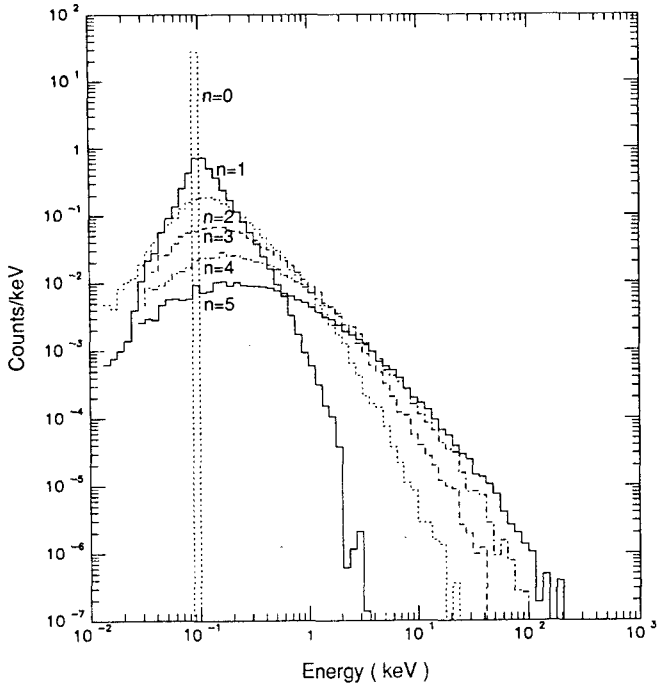


**Fig. 3.** Contribution of the scattered component to the energy spectra. The monochromatic photons are scattered in the plasma shell with the scattering depth $\tau=1$. The number $n$ denotes frequency of the scattering. The normalization of the spectra is same as in Fig. 2.

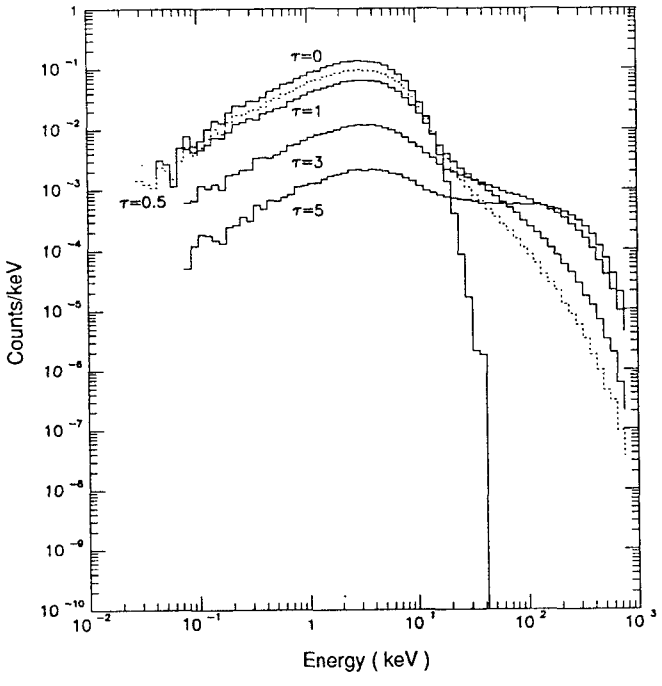


**Fig. 4.** Comptonized spectra of the blackbody of $kT_b=2$keV emerging from the spherical shell. The simulation parameters are same as in Fig. 2.

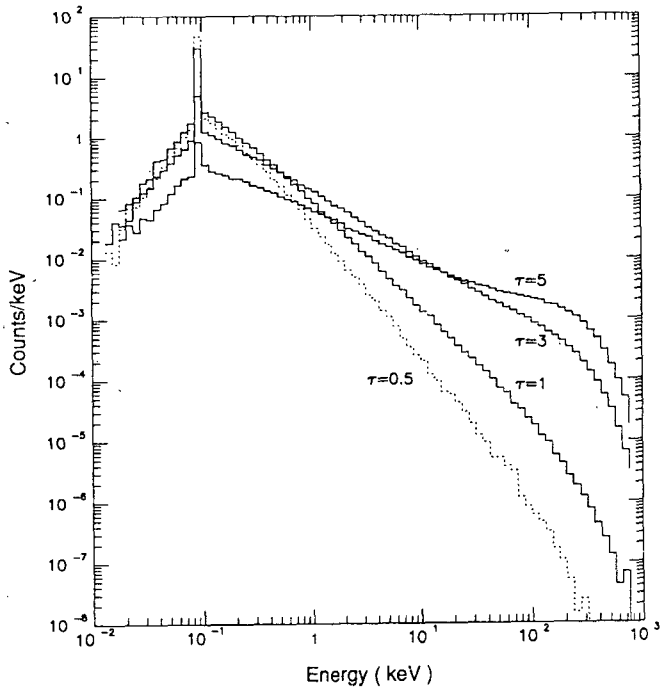


**Fig. 5.** The energy spectra escaping from the plasma sphere. The simulation parameters are same as in Fig. 2. The individual spectrum is normalized by the input photons.

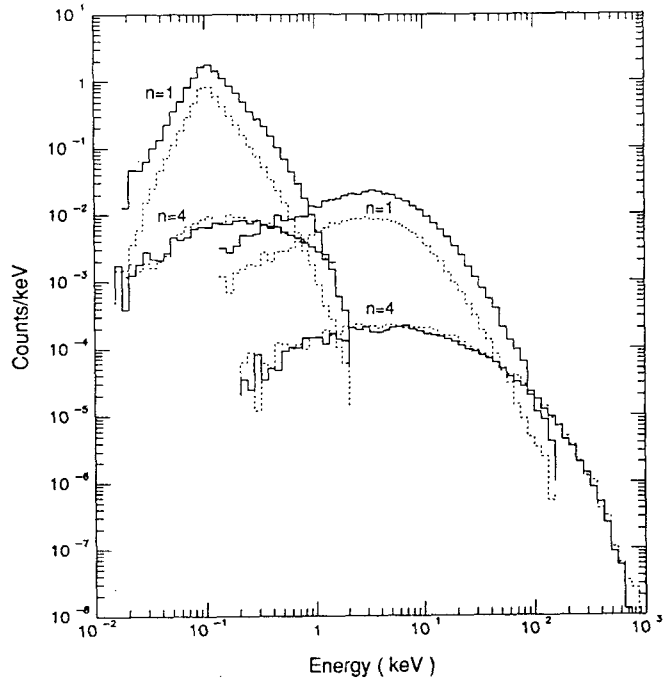


**Fig. 6.** The emergent spectra according to the difference of the plasma geometries and to the initial input spectra. The solid curves and the dotted curves are the spectra escaping from the sphere and the shell, respectively. The spectra represented in the left and the right of the Figure are correspond to the Comptonization of the monochromatic photons of $E_0=0.1$keV and to that of the blackbody of $kT_b=2$keV, respectively.

spectra show slightly softer than that of the shell model over the same $\tau$ (see also Table 1). The direct comparison of geometrical effect is made for $\tau=0.5$. The solid curves and the dotted curves in Fig. 6 are the spectra escaping from the sphere and the shell, respectively. The spectra represented in the left and the right of Fig. 6 are correspond to the Comptonization of the monochromatic photons of $E_0=0.1$keV and to that of the blackbody of $kT_b=2$keV, respectively. The Figure implies that each spectral component is independent of the geometry of the scattering medium, while the relative contribution of $n$ scattered components depends on the geometry. In the spherical shell geometry, the probability of backscattering into the neutron star after being scattered 4 times is very low, while the probability after being scattered one time is relatively high. Thus, the contribution of 4 times scattered component is almost same in both the geometries, but it is different in the case

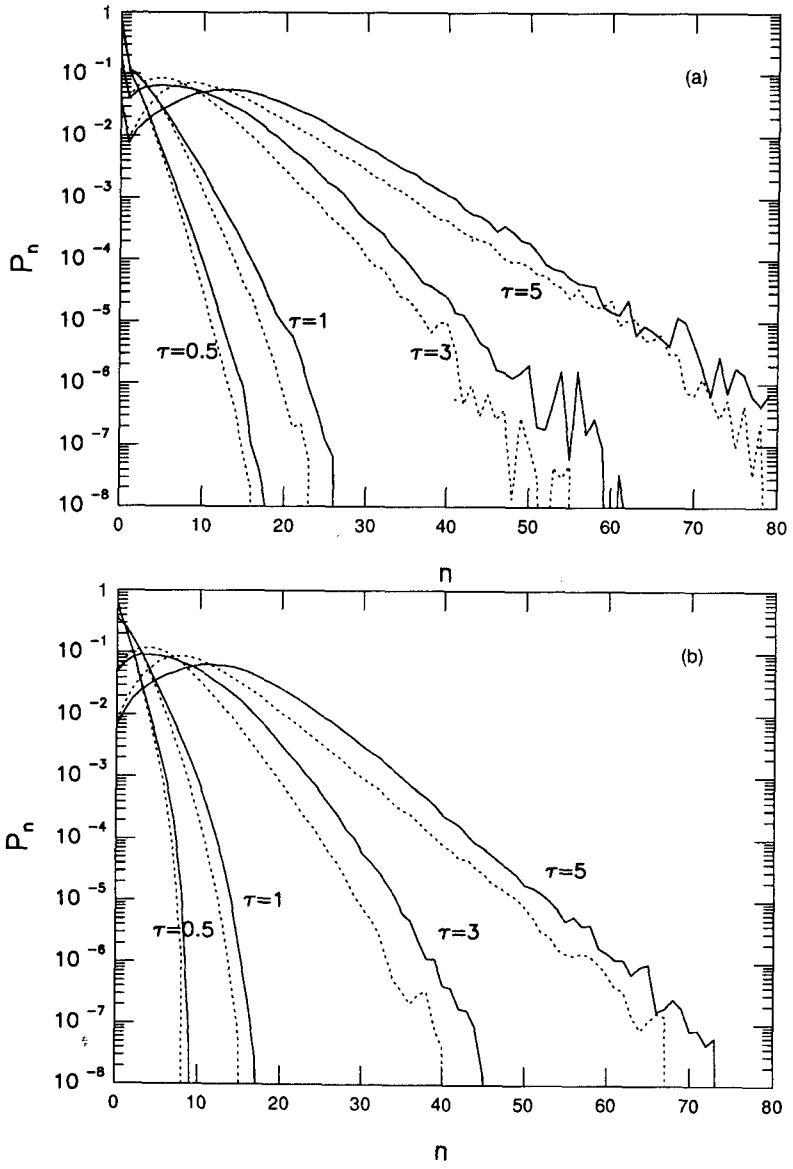


**Fig. 7.** The escape probability of a photon from the plasma after being scattered $n$ times. The solid curves and the dotted curves correspond to the monochromatic case and to the blackbody, respectively. The geometries of the scattering mediums are the spherical shell (a) and the sphere (b), respectively. The escape probability is normalized, and the absorbed photons are not considered in the normalization.

of one time scattered component. The escape probability $P_n$ after being scattered $n$ times is shown in Fig. 7. The obtained solid curves and dotted curves correspond, respectively, to the monochromatic case and to the blackbody. For the same $\tau$, the slope in the shell (Fig. 7a) is less steeper than the case of the sphere (Fig. 7b). $P_n$ follows the asymptotic series $P_{n+1}/P_n = const$ for the sufficiently large scattering depth $\tau > 3$. This will be discussed in the following section.

## IV. DISCUSSION

In the previous section, Monte Carlo method has been used to understand qualitatively the observed X-ray spectra of LMXBs. Among the observed LMXBs, the power-law components is outstanding only for the low luminosity state (Parmar, Stella & White 1986; King & Lasota 1987). King & Lasota (1987) have suggested that a boundary layer where the accretion disk interacts with the neutron star surface is geometrically thin (geometrical depth$\ll R_0$), at the higher luminosity state of LMXBs. However, the boundary layer becomes hotter and thicker, as the luminosity declines. Thus the assumed shell geometry of the present work is not unresonable to apply for the low luminosity state of LMXBs.

We have showed that the power-law component is explained well with the present model. The spectral index $\alpha \sim 2$ obtained in the model spectra of $\tau = 0.5$ is consistent with that of the typical observation for many LMXBs (White, Stella & Parmar 1988). The X-ray spectra obtained from the spherical shell are very similar to that of the sphere, except the spectral hardness. We suggest that the spectral difference is due to the relative contribution of the multiple scattering component. This fact agrees with the behavior of the escape probabilities shown in Fig. 7.

If we assume that $\psi_0(E)$ and $\psi_n(E)$ are, respectively, the initial photon spectrum and the spectrum of the scattered components, then the output spectrum $\psi(E)$ can be approximated by (Illarinov *et al.* 1979; Lightman & Rybicki 1980; Nishimura, Mitsuda & Itoh 1986)

$$\psi(E) = \sum_{n=0}^{\infty} P_n \psi_n(E). \tag{4}$$

We expect that photons can be scattered into all directions after a number of scatterings, since the information for the initial angle would be lost. In this condition, $P_n$ approaches asymptotically to a series in the limit of $n \to \infty$,

$$P_{n+1}/P_n = 1 - e^{-\tau_{eff}} \text{ for large } n, \tag{5}$$

where $\tau_{eff}$ is the effective scattering depth to be determined by the probability of further scattering. To simplify, we assume that the above equation is valid for $n \geq n_0$. If then the solution of Eq. (5) could be expressed as (Nishimura, Mitsuda & Itoh 1986)

$$P_n = P_{n_0} (1 - e^{-\tau_{eff}})^{n-n_0} \text{ for } n \geq n_0. \tag{6}$$

The contribution of $n$ scattered component decreases exponentially with increasing $n$ for sufficiently large $\tau$. The asymptotic value of $P_{n+1}/P_n$ is independent of the initial X-ray photons, as can be seen in Fig. 7. The effective scattering depths $\tau_{eff}$ calculated for $\tau = 5$ is 1.75 for the spherical shell and 1.51 for the sphere.

Nishimura, Mitsuda & Itoh (1986) have suggested that the ratio $P_{n+1}/P_n$ approaches an asymptotic value for large $n$ irrespective of the geometry of the scattering medium. However, we insist that the asymptotic value of $P_{n+1}/P_n$ estimated in this study is closely related with the geometry of the scattering medium, taking into account the angular dependence of the scattering cross-section. In contrast to this dependence, the functional form of $\psi_n(E)$ is independent of the geometry as seen in Fig. 6.

## V. CONCLUSION

In this paper, we have performed the Monte Carlo simulation with the spherical shell plasma to study on the Comptonization process of the LMXBs. From the simulation, we find that the hot plasma reproduces resonably well the power-law component observed in the low-luminosity of the LMXBs. In addition, we recognize that the Wien spectral features appear when the plasma is optically thick, especially in the high energy range $E \gtrsim$ 100keV. The direct comparison of geometrical effects shows that each scattered component is independent of the plasma geometry, while the relative contribution depends on the geometry. In the limit of $n \rightarrow \infty$, the escape probability $P_n$ approaches the asymptotic form, which depends on the geometry of scattering medium rather than on the initial photon spectrum.

## ACKNOWLEDGEMENT

The authors wish to thank Prof. Myeong-Gu Park for careful reading and helpful comments on the manuscript. This work was supported in part by the Basic Research Project 93-5100-002 of the Korea Astronomy Observatory.

## REFERENCES

Babuel-Peyrissac, J. P. & Rouvillois, G., 1969, J. Phys., 30, 301
Felten, J. E. & Rees, M. J., 1972, A&A, 17, 226
George, I. M. & Fabian, A. C., 1991, MNRAS, 249, 352
Haardt, F., Done, C., Matt, G. & Fabian, A. C., 1993, ApJ, 411, L95
Hanawa, T., 1990, ApJ, 355, 585
Katz, J. I., 1976, ApJ, 206, 910
King, A. R. & Lasota, J. P., 1987, A&A, 185, 155
Kompaneets, A. S., 1957, Sov. Phys. JETP, 4, 730
Landau, L. D. & Lifshits, E. M., 1976, in the Classical Theory of Fields 4$^{th}$ ed, (New York: Pergamon)
Langer, S. H., Ross, R. R. & McCray, R., 1978, ApJ, 222, 950
Lightman, A. P. & Rybicki, G. B., ApJ, 236, 928
Illarinov, A., Kallman, T., McCray, R. & Ross, R., 1979, ApJ, 228, 279
Matt, G., Perola, G. C. & Piro, L., 1991, A&A, 247, 25
Nishimura, J., Mitsuda, K. & Itoh, M., 1986, PASJ, 38, 819
Parmar, A. N., Stella, L. & White, N. E., 1986, ApJ, 304, 664
Ponman, T. J., Foster, A. J. & Ross, R. R., 1990, MNRAS, 246, 287
Pozdnyakov, L. A., Sobol', J. M. & Sunyaev, R. A., 1983, Sov. Sci. Rev., E2, 189
Shapiro, S. T., Lightman, A. P. & Eardley, D. M., 1976, ApJ, 204, 187
Sunyaev, R. A. & Titarchuk, L. G., 1980, A&A, 86, 121
White, N. E., Stella, L. & Parmar, A. N., ApJ, 324, 363
Zeldovich, Y. B. & Shakura, N. I., 1969, Sov. Astron., 13, 175